# Maximum Harvesting Power Algorithm Considering Temperature Variation in Magnetic Energy Harvester

Bumjin Park, Sungryul Huh, Haerim Kim, Jongwook Kim, Yujun Shin, Seongho Woo, Dongwook Kim, Ki-Bum Park, Okhyun Jeong, Ja-il Koo and Seungyoung Ahn, *Senior Member, IEEE*

***Abstract*— A major challenge for practical magnetic energy harvesting (MEH) applications is achieving stable harvested power with high power density under a wide range of temperature variation. The amount of power harvested from the MEH is sensitive to ambient temperature because the characteristics of the magnetic material are greatly affected by temperature. From a practical point of view, previous studies have limitations because they do not consider thermal effects at all. In order to address the issue, this paper proposes a novel control algorithm for maximum harvested power in MEH by considering dynamic changes in temperature for the first time. In this paper, a robust MEH design method based on a temperature-dependent B-H curve model is proposed, which considers the effect of temperature variation on the magnetic core. The thermal effect was considered at the design level for the first time in MEH. The theoretical analysis based on the proposed B-H curve model showed that the nonlinearity of the magnetic material could be accurately predicted according to temperature changes. Based on the above analysis, it was possible to extract the maximum harvested power and to predict the changes in magnetic saturation point under a wide range of temperatures. Experimental results showed that the proposed design method had a 26.5% higher power density than the conventional method, which does not consider the temperature effect.**

***Index Terms*—Magnetic energy harvesting, magnetic saturation, thermal effect, magnetic material**

## I. Introduction

With the recent increase in global demand for electrical energy, power systems have become larger and more complex to meet growing energy consumption. This complexity is expected to increase the stress, disturbances, and vulnerability of the power system. To tackle these problems and maintain high reliability, it is essential to perform constant inspections and preventive maintenance of the power system for fault-free operation [1].

Typically, utility assets are exposed to damage from natural hazards such as fallen trees, wildfires, and so on. At the same time, most maintenance tasks still rely on manpower. Since most utility assets involve high voltage and high current environments, the maintenance and inspection work is extremely risky for technical personnel.

To solve these issues, various types of applications have been developed, including wireless sensors [2], [3], inspection robots [4], [5] and unmanned aerial vehicles [6]. These devices enable utility operators to maintain high reliability and oversee a wide region. In addition, human exposure to dangerous high voltage environments can be eliminated and maintenance costs are reduced. Although these devices are efficient, they require an independent power source for continuous operation. Indeed, it is impossible to connect wire physically because of the large potential difference near high voltage power lines. For this reason, most of the devices heavily rely on battery power, which requires periodic replacement. To solve the limitations posed by present power supplies, energy harvesting is being studied as a practical solution, to make the system self-sustainable instead of dependent on battery power.

There are various candidate energy sources for harvesting near power lines. In [7], a number of energy harvesting methods were compared from a practical point of view. Referring to the above paper, our research concluded that MEH was a suitable method near power lines in three major respects. Firstly, MEH has high reliability as a power supply. The MEH is not affected by weather conditions, so it can be a stable power supply for tens of watts level applications beyond sensor devices. Secondly, the MEH has a high power density compared to other energy sources [8]. This means that the effect on the power line, such as additional undesired sag due to the weight of the harvester, can be minimized. Finally, unlike other harvesting methods, MEH has the advantage that it can be applied to indoor environments, such as underground transmission lines. Above them, power density is the most critical design factor in MEH, so many related studies have been conducted [8]-[14].

One major hurdle in MEH design is the degradation in power density due to magnetic saturation. When the MEH is operated in the saturation region, there is no change in magnetic flux density, and harvested power is reduced to zero. For this reason, previous studies have focused on preventing or overcoming saturation. In [10], the threshold current, which is current at which the magnetic core is saturated, was determined based on the maximum flux density of the magnetic material. In [11], the output was improved by using the saturation region in reverse. It was confirmed that the maximum output is generated in the region called the ‘soft saturation region’. To operate in this

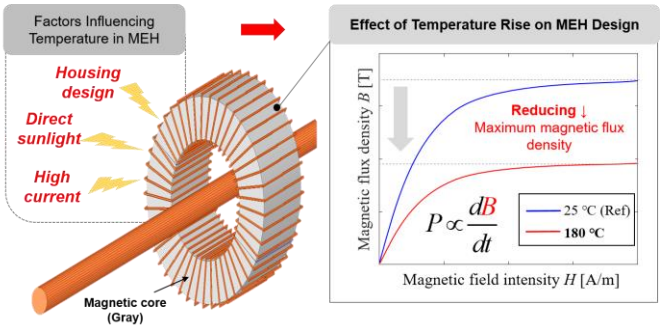


Fig. 1. Effect of temperature variables on MEH output performance.

region, the load voltage is controlled based using *B-H* curve modeling. In [12], the saturation was overcome by using a reverse magnetic field through an additional power circuit. To manipulate the magnetic field, the optimal load voltage was analyzed based on the previously mentioned *B-H* curve model. To summarize the previous research, the power density was improved by adjusting the load voltage based on the *B-H* curve model.

However, from a practical point of view, MEH is easily affected by temperature effects depending on the weather condition, installation location, primary current intensity, and housing design. In particular, the magnetic core is sensitive to temperature. This may produce a variation in the magnetic flux density as shown in Fig. 1, which may affect the output performance as a result [13]. If the effect of temperature is not considered at the design level, the saturation voltage will be set higher than the expected value. This means that the magnetic core can become saturated due to temperature. As a result, the optimal load voltage will be incorrectly predicted, and output power may be significantly reduced.

In [13], resonance condition was used by adding a compensation capacitor to minimize reactive power. However, as the temperature rises, the impedance matching condition changes and the output power is rather reduced. These challenges have not yet been addressed. In any case, from the practical point of view, it is important to consider the effect of temperature rise for maximum power extraction in MEH design.

In this paper, we propose a robust MEH design method with improved power density using control algorithm considering magnetic saturation induced by temperature rise. For the first time, we analyze the MEH for maximum power extraction by considering magnetic saturation in relation to the effect of temperature variation. In order to consider temperature effects in MEH design, circuit parameters and saturation conditions were obtained through temperature-dependent *B-H* curve modeling. To confirm the effect of temperature variation, ferrite was used as the magnetic material and harvested power was measured under different temperature conditions ranging from 25 to 200 ℃. This range is based on the temperature characteristics of ferrite PL-7 [15]. With the aid of the proposed algorithm, the maximum harvested power of MEH under different temperature conditions improved compared to conventional methods.

Consequently, our research differs from and extends conventional works [2]-[18] in many respects:

1) Modeling and procedures for maximum harvested power were developed while considering temperature effects
2) Improved power density was obtained under different temperature conditions, compared to the conventional model

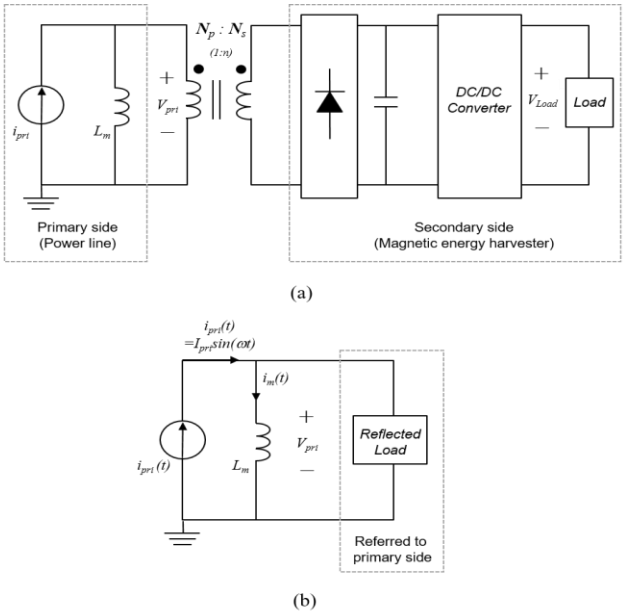


Fig. 2. Schematic for magnetic energy harvesting system. (a) Simplified equivalent circuit of power line and magnetic energy harvester. (b) Approximated equivalent circuit reflected to primary side.

The paper is organized as follows: Details on the output power model are given in Section II. Section III gives a detailed description of the proposed design methodology. Section IV presents a detailed description of the measurement setup and experiment results. Finally, the conclusions are given in Section V.

## II. Theoretical Analysis for Maximum Harvested Power in MEH

An equivalent circuit was developed as shown in Fig. 2(a). To simplify the circuit analysis, we expressed the magnetizing inductance $L_m$ and transformer model instead of using the mutual inductance model [7]. The super-capacitor was connected to the core as a load, which can be considered to be a constant dc voltage. The leakage inductance and core-loss components were neglected because the power line current is modeled as the current source. For simplicity, all components are reflected on the primary side as shown in Fig. 2(b). In this case, the primary voltage $V_{pri}$ is the important factor for determining harvested power in the MEH [8].

### A. Analysis of Load Voltage and Harvested Power

The formulas for averaged harvested power $P_o$ can be expressed as follows [14]:

$$P_o = \frac{1}{0.5T_p}\int_{t_s}^{t_s+0.5T_p} V_{pri}\cdot\frac{(i_{pri}(t)-i_m(t))}{N_s}\,dt \qquad (1)$$

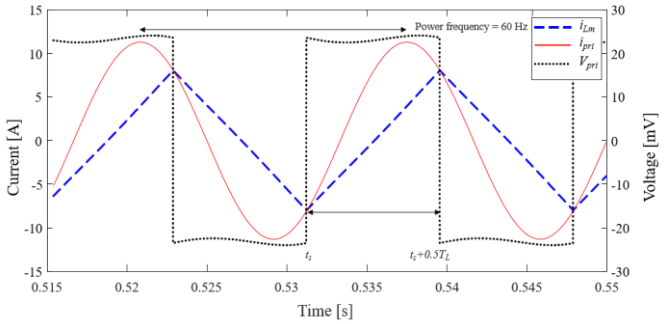


Fig. 3. Time-domain waveform relation between magnetizing current and primary side current.

where $T_P$ is the power line period and $t_s$ is the start time of transferring current to load, respectively. $N_s$ is the number of harvester winding turns.

The waveforms of the primary current $i_{pri}$ and magnetizing current $i_m$ are shown in Fig. 3. The transfer of current to load is determined according to the difference between $i_{pri}$ and $i_m$. To calculate $t_s$, we can use the relationship in the flux quality in the inductor. Based on volt-second balance, the ripple of $i_m$ can be expressed as follows:

$$\Delta i_m = \frac{\int_{t_s}^{t_s+0.5T_p} V_{pri}\, dt}{L_m} \cong \frac{V_{pri} \cdot 0.5T_p}{L_m} \tag{2}$$

Since $i_{pri}$ and $i_m$ have the same value at $t_s$ as shown in Fig. 3, the peak value of the magnetizing current $i_m^{pk}$ can be obtained as follows:

$$i_m^{pk} = I_{pri} \sin(\omega_o t_s) = -i_m(t_s) \tag{4}$$

where $\omega_o$ is the angular frequency on the primary side and $I_{pri}$ is the peak value of the power line current.

Equation (2) can be used to calculate the $i_m^{pk}$ because the offset value of $i_m$ is zero. Taking this into account, $i_m^{pk}$ can be expressed as half of the ripple of the magnetizing inductance current.

Then, the $i_m^{pk}$ simply become

$$i_m^{pk} = 0.5 \cdot \Delta i_m = \frac{V_{pri} \cdot T_p}{4L_m} \tag{5}$$

In summary, $t_s$ can be determined by substituting (5) for $i_m^{pk}$ as follows:

$$t_s = -\frac{1}{\omega_o} \sin^{-1}\left(\frac{V_{pri} \cdot T_p}{4L_m I_{pri}}\right) \tag{6}$$

Based on (6), if the magnetic core is fixed, the $t_s$ depends on not only the intensity of the primary current but also the load voltage across.

Taken together, $P_o$ can be expressed by substituting (6) for $t_s$ in equation (1) as follows:

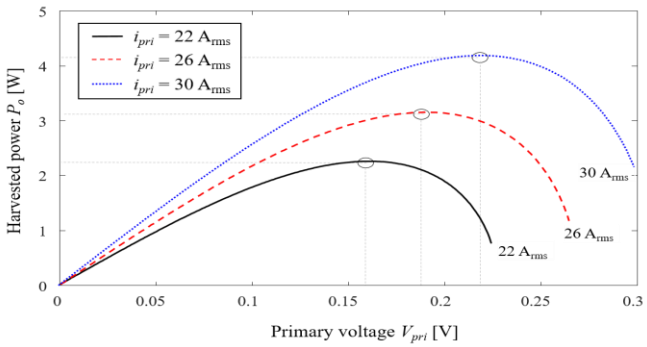


Fig. 4. Harvested output power response with a load voltage according to primary side current.

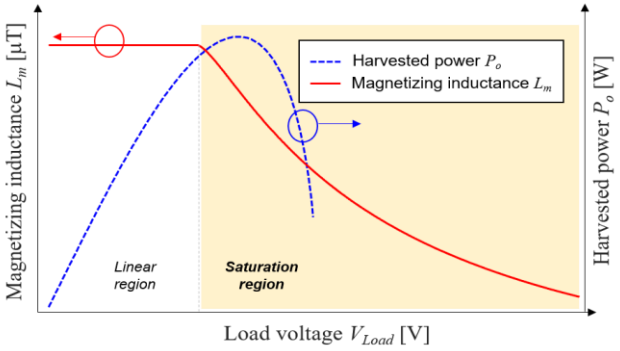


Fig. 5. Harvested output power and magnetizing inductance response with a load voltage.

$$\begin{aligned} P_o &= \frac{2V_{pri}I_{pri}}{T_p N_s} \int_{t_s}^{t_s+0.5T} \sin(\omega_o t)\, dt \\ &= \frac{2V_{pri}I_{pri}}{\pi} \cos(\omega_o t_s) \end{aligned} \tag{7}$$

Based on (6) and (7), if $I_p$ and $L_m$ are fixed with a constant value, the $P_o$ only depends on the load voltage across. To calculate the primary voltage for harvesting the maximum power $V_{pri,max}$, equation (7) is differentiated with respect to $V_{pri}$ as follows:

$$\left.\frac{\partial P_o}{\partial V_{pri}}\right|_{n=V_{pri,\max}} = 0 \Rightarrow V_{pri,\max} = \frac{4\sqrt{2}L_m I_{pri}}{T_p} \tag{8}$$

Thus, the maximum harvested power $P_{o,m}$ can be derived from (6)-(8) as follows:

$$P_{o,\mathrm{m}} = \frac{4L_m}{\pi T_p} \cdot I_{pri}^{\ 2} \tag{9}$$

According to equation (9), $P_{o,m}$ increases with the intensity of the power line current and magnetizing inductance. Fig. 4 illustrates an example with $L_m$ = 30.4 μH and frequency = 60 Hz according to different power line currents. As the $i_{pri}$ increases, the load voltage for maximum harvested power also increases according to equation (8)-(9).

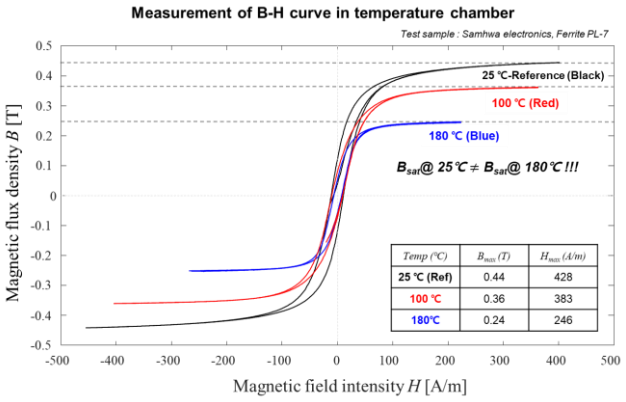


Fig. 6. Temperature dependence of the magnetic material (ferrite) through measurement of *B-H* curve.

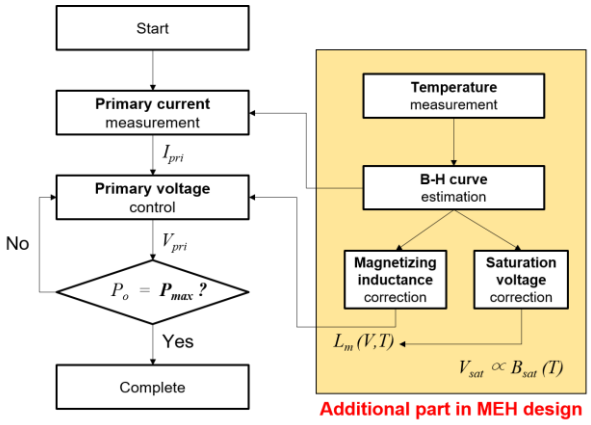


Fig. 7. Proposed maximum power extraction algorithm by considering temperature dependence of magnetic material.

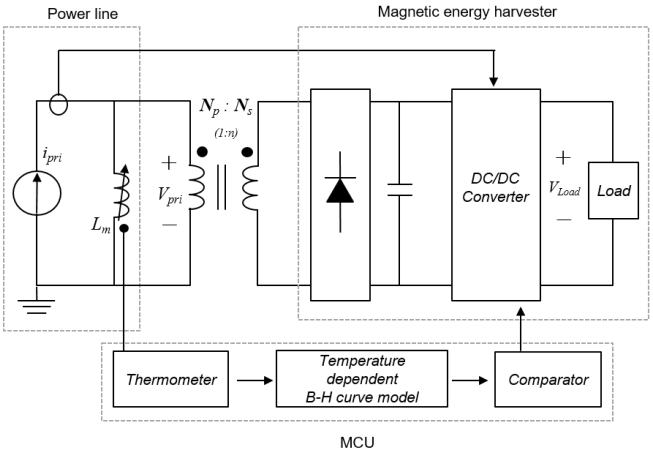


Fig. 8. Block diagram of proposed maximum power extraction control scheme by considering temperature variation

### *B. Design Consideration: Magnetic Saturation Effect in Magnetic Core*

Equation (9) is helpful to confirm the relationship between the design parameters. However, from a practical point of view, magnetic saturation should be considered in the MEH design. The environment in which the MEH is installed can include irregular current flows and has a very wide current range. In other words, the magnetic core can be saturated by extremely strong magnetic field intensity.

When the MEH is operated in the saturation region, $P_o$ is drastically reduced because there are no changes in magnetic flux density and the reduction of the $L_m$ value, as shown in Fig. 5. Here, it is assumed that the primary voltage and load voltage are the same due to the super-capacitors across the load.

As the primary voltage across the load increases, the $L_m$ no longer maintains a constant value. To determine the saturation voltage $V_{sat}$, a voltage second balance between the maximum flux is set by the saturation flux density $B_{sat}$ for the magnetic core and the applied voltage is integrated over half-period.

$$\int_0^{\frac{T_p}{2}} V_{sat}\, dt = 2B_{sat}A_eN_p \tag{10}$$

where the cross-sectional area of the magnetic core and the number of primary winding turns are expressed as $A_e$ and $N_p$, respectively.

According to [11], the coefficient "2" before $B_{sat}$ on the left side means that the magnetic flux density is changed from one end of the *B-H* curve($-B_{sat}$) to the other end of the *B-H* curve($+B_{sat}$), which results in a total change of $2B_{sat}$ in a half period.

To prevent saturation in the magnetic core, $V_{pri}$ must be determined under the $V_{sat}$, which can be expressed as follows [14]:

$$V_{sat} = \frac{4A_eB_{sat}N_p}{T_p} \tag{11}$$

However, MEH can also be saturated with temperature rises. In general, the saturation magnetic flux density characteristic of a magnetic material decreases with rising temperature as shown in Fig. 6. When the temperature rises, the above equations (1)-(11) are invalid due to the changes in the properties of magnetic material, such as $L_m$ and $B_{sat}$.

If the temperature effect is not taken into account in the MEH design, as in the conventional design method, the magnetic core may be easily saturated and operated in the hard saturation zone. As a result, heat is generated due to increasing core loss and the power density may be reduced. Until now, there has been no research considering these effects. So, it is necessary to consider the effect of temperature rise for maximum power extraction in the MEH design.

## III. Proposed Harvesting Method for Considering the Saturation Effect Due to Temperature Changes

### *A. Proposed Algorithm for Maximum Power Extraction in MEH by Considering Temperature Dependence*

The conventional method of maximum power extraction aims to prevent saturation by controlling the primary voltage, which can be derived from (8) and (11). From a practical point of view, this is not effective since the variation in magnetic flux density with rising temperature will cause a change in $V_{sat}$. As a result, the output performance of the MEH is degraded by operating in the hard saturation region.

If the change in magnetic flux density with temperature changes can be predicted, magnetic saturation can be prevented and the power density can be increased compared to the conventional design method. A design method to solve the above challenges related to temperature dependence in MEH is proposed, as shown in Fig. 7.

In the conventional methods, the maximum power is extracted by measuring the line current and adjusting the load voltage accordingly. According to equation (8), the primary voltage is determined for harvesting the maximum power. However, the conventional design method [11], [12] do not consider the temperature dependence of the magnetic material in the magnetic core. So it is not robust to variable temperature conditions, and as a result, the power density is greatly reduced due to incorrect selection of the optimal load voltage.

In order to solve the above problems, the *B-H* curve information according to temperature changes was estimated through the proposed modeling. The additional part added to the conventional algorithm is marked in yellow. In the content added to the existing algorithm, based on the proposed *B-H* curve model, which is temperature-dependent, $B_{sat}$ and $L_m$ are re-estimated and reflected in the MEH design. By adjusting refined $V_{pri,max}$, maximum power can be harvested according to the temperature change. As a result, power density can be improved compared to the existing design method.

The control scheme for maximum power extraction is shown in Fig. 8. The variable $L_m$ is controlled by the variation of $V_{pri}$ through DC/DC converter. However, in this case, the characteristic of the magnetic material is changed according to magnetic core's temperature. Therefore, the control scheme is needed to become robust system against disturbance such as variation of temperature.

In order to confirm the magnetic core's temperature changes, the temperature is measured using a thermometer. Based on the measured temperature, a *B-H* curve model is selected according to temperature. Though the comparator, the error between the reference voltage and the measured $V_{pri}$ is confirmed and saturation voltage is reset by considering temperature dependence. Here, reference voltage is $V_{pri}$ according to temperature variation. Taken together, the maximum power is extracted by adjusting the $V_{pri}$ through DC/DC converter.

### *B. Proposed Theoretical Model for Temperature Dependence in the B-H curve*

In this section, the principle of the proposed theoretical model of the *B-H* curve is going to be explained. According to the previous analysis based on equations (1)-(11), $B_{sat}$ and $L_m$ are important design factors when determining the power density of the MEH. The two design parameters are determined using the *B-H* curve of the magnetic material.

According to [11], the *B-H* curve can be modeled with the "arctangent" function as follow:

$$B = B_{sat} \cdot \frac{2}{\pi} \cdot \arctan\left(\frac{H}{\alpha}\right) \tag{12.a}$$

$$H = \frac{I_m}{2\pi R_{in}\alpha} \tag{12.b}$$

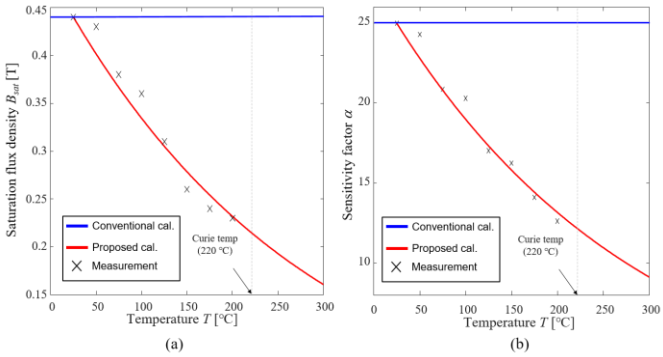


Fig. 9. Numerical calculations and measurement results according to temperature variation. (a) Saturation flux density response with temperature changes. (b) Sensitivity factor response with temperature changes.

where the magnetic flux density, the magnetic field intensity, and the inner radius of the magnetic core are expressed *B*, *H*, and $R_{in}$, respectively.

'$2/\pi$' is a scaling factor, which is used to normalize the arctangent function to 1, when the magnetic core is saturated. The '$\alpha$' describes the sensitivity factor in the linear region and determines relative permeability, which affects the $L_m$ value [11]. However, one limitation of equation (12.a) is that $B_{sat}$ is a constant value, and thus cannot accurately reflect the change in the properties of the magnetic material as the temperature varies. As described in the previous section, the main difference is the reduction of $B_{sat}$ as the temperature rises. For example, at 175 ℃, $B_{sat}$ decreases by 55% compared to room temperature. Besides, the gradient (= relative permeability) changes in the linear region also have an effect. Therefore, it is necessary to model the changes in $B_{sat}$ and $\alpha$ with the temperature changes.

To solve the above problems, the proposed theoretical model was based on a combination of physical and empirical approaches to represent the experimental data-related temperature. The $B_{sat}$ response with temperature is as shown in Fig. 9(a). In this figure, $B_{sat}$ decreases as the temperature rises, which means that the magnetic core is more easily saturated as temperature rises. In other words, the MEH can be saturated not only by the magnetizing current but also by the rising temperature.

To describe the reductions of $B_{sat}$ with increasing temperature, an exponential decay model is used, as follows:

$$B_{sat}(T) = B_{sat} \cdot e^{-\left(\frac{T-T_{ref}}{T_{ref}}\right)} \tag{13}$$

where $T_{ref}$ is room temperature, 298 K (=25 ℃) and $T$ is the ambient temperature.

The '$\alpha$' response with temperature variation is as shown in Fig. 9(b). To describe the variation in '$\alpha$' with temperature rise, '$\alpha$' can also be expressed as a function of temperature with an exponential decay model, as follows:

$$\alpha(T) = \alpha_{ref} \cdot e^{-\left(\frac{T-T_{ref}}{T_{ref}}\right)} \tag{14}$$

where $\alpha_{ref}$ is the sensitivity factor in room temperature.

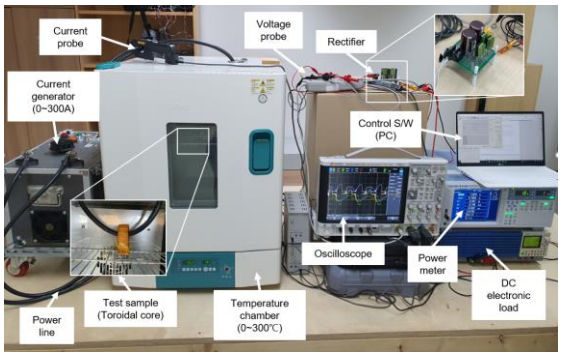


Fig. 10. Experimental setup by considering temperature effect.

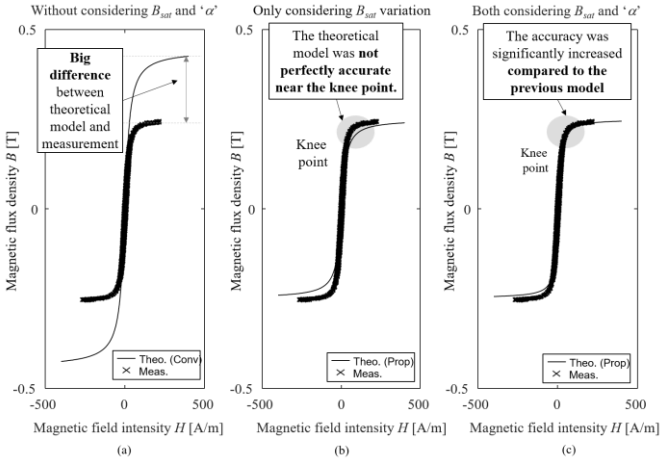


Fig. 11. Numerical calculations and measurement results with 175 ℃. (a) Large gap between theoretical model and measurement (w/o considering $B_{sat}$ and $\alpha$ (b) small error between theoretical model and measurement near knee point (w/ only considering $B_{sat}$ variation (c) Accurate theoretical model with improved accuracy (w/ both consider $B_{sat}$ and $\alpha$)

Using the proposed model, equations (11) and (12) can be replaced by substituting (13) for $B_{sat}$. Similarly, equation (12) can be also replaced by substituting (14) for '$\alpha$'. As a result, the accuracy can be significantly improved compared to the existing model.

## IV. Experimental Results

Based on the above analysis, the feasibility of the proposed design method was tested using experimental results. The magnetic core was manufactured in a toroidal form by laminating a sheet-type Mn-Zn ferrite PL-7 [15]. The detailed parameters of the magnetic core are listed in Table I.

To verify the proposed method, an experimental setup was built as shown in Fig. 10. To confirm the temperature effect for the MEH design, the magnetic core and power line were placed in a temperature controlled chamber. The temperature range in the chamber was from 25 to 200 ℃. In the constant voltage condition, the load voltage was adjusted through electronic load (KIKUSUI PLZ1004W). To compare the results of the proposed model and the measurement results, the *B-H* curve can be extracted based on IEEE standard [16]. For the first time, to consider the temperature dependence, the test sample was

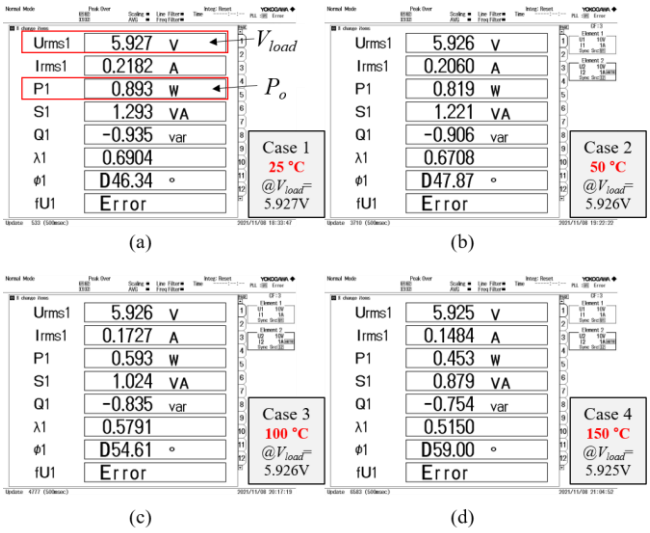


Fig. 12. Comparisons of the experimental result according to temperature different conditions when $I_{pri}$ = 60.1 A. (a) Case 1: $V_{Load}$ = 5.927 V, $T$ = 25 ℃. (b) Case 2: $V_{Load}$ = 5.926 V, $T$ = 50 ℃. (c) Case 3: $V_{Load}$ = 5.926 V, $T$ = 100 ℃. (d) Case 4: $V_{Load}$ = 5.925 V, $T$ = 150 ℃.

TABLE I
DETAILED PARAMETERS OF MAGNETIC CORE

| Parameters | Quantity |
|---|---|
| Magnetic core material | Ferrite PL-7 [15] |
| Magnetic core information | Fig. 6 |
| Number of harvester winding turns | $N_s$ = 114 |
| Magnetic core height | 25 mm |
| Outer radius (with/without insulation sheet) | $R_{out}$ = 38.5/38.2 mm |
| Inner radius (with/without insulation sheet) | $R_{in}$ =22.5/22.2 mm |
| Saturation flux density | $B_{sat}$ = 0.44 T @25 ℃ |
| Power frequency | 60 Hz |

placed in a temperature chamber. The temperature range in the chamber was from 25 to 200 ℃. Ferrite was selected as the magnetic material, and the magnetic core was manufactured in a toroidal form by laminating a sheet type.

Fig. 11 illustrates measurement examples with $T$ = 443 K (=175 ℃) compared to the conventional model. Fig. 11(a) shows a significant difference between the experimental results and the theoretical model. The cause of the error is that the change in $B_{sat}$ according to temperature was not reflected in the model [11]. To address the above problems, $B_{sat}$ variation according to temperature was reflected in the model, as shown in Fig. 11(b). The accuracy of the theoretical model was significantly increased compared to the previous model, but it was not perfectly accurate near the knee point. The shaded circular area expressed in gray indicates the knee point of the magnetic material. Finally, Fig. 11(c) shows the proposed model which considers both $B_{sat}$ and '$\alpha$' in order to reflect the change in permeability near the knee point. The main difference from the theoretical model applied in Fig. 11(b) is that the change in permeability at the knee point is considered. Using the proposed model, the magnetizing inductance can be more accurately extracted than when using the existing model under variable temperature conditions.

Fig. 12 shows the $P_o$ measured with the power analyzer (YOKOGAWA WT1800) under varying load voltage according to different temperature conditions of 25, 50 100, and

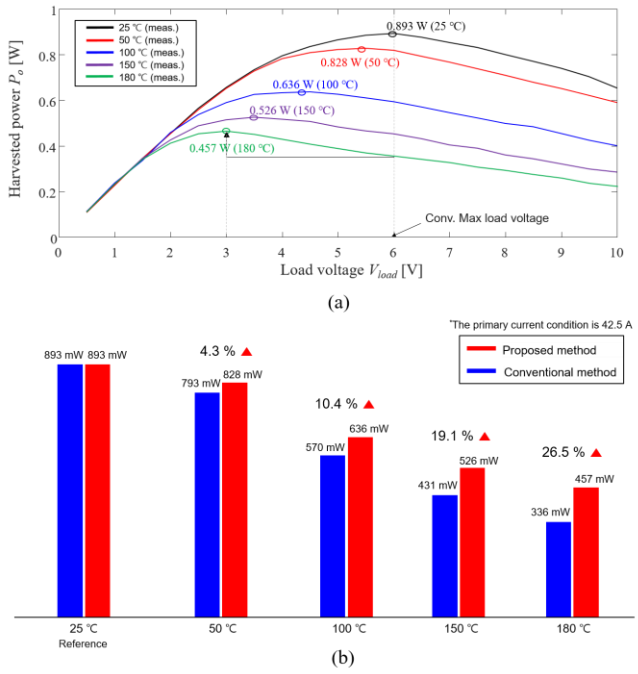


Fig. 13. Comparisons of proposed and conventional method according to load voltage and temperature. (a) Harvested power according to load voltage (b) maximum harvested power according to temperature.

150 ℃, respectively. At 25 ℃, it has a $V_{L,max}$ of 5.927 V, but the maximum $P_o$ decreases as the temperature rises. The reason is that as the $L_m$ value with temperature rises, $V_{L,max}$ also changes. To compensate for this, the proposed design method adjusts the $V_L$ according to temperature, and tracks the point of maximum $P_o$.

Fig. 13(a) shows the $P_o$ response with a $V_L$ according to temperature. When the temperature in the chamber increases, the maximum $P_o$ gradually decreases. Interestingly, $V_{L,max}$ and $V_{sat}$ also decrease with rising temperature. This means that the MEH can operate under saturation conditions depending on the temperature. If the effect of temperature is not taken into account, as with the conventional methods [17], [18], there is a possibility that it will operates in the hard saturation section, and as a result, the output of the MEH will drastically decrease, and the reactive power increase.

Fig. 13(b) compares the maximum $P_o$ with the conventional method according to temperature changes. The red bar indicates the maximum $P_o$ when the proposed method is applied. The blue bar represents the maximum $P_o$ of the MEH using the conventional method, which ignores the temperature effect. By considering the temperature variation effect the proposed design method had a 26.5% higher output performance than the conventional method. This tendency is attributed to the reduction in the change in magnetic flux density in the magnetic core as the temperature increases.

## V. Conclusion

In this paper, a robust MEH design method which considers the effect of temperature variation was proposed, based on temperature-dependent *B-H* curve modeling. The proposed design method extracts the circuit parameter by considering the temperature effect, resulting in a more robust and practical design method compared to the conventional method. Saturation conditions according to temperature in the MEH design were proposed and applied for the first time.

In the proposed algorithm, only the temperature information in the magnetic core was required, which decreases complexity and improves reliability. The proposed method is expected to contribute to improving power density without using additional magnetic material or number of windings. The proposed concept was demonstrated experimentally to validate the theoretical analysis. Experimental results show that the proposed design method resulted in a 26.5% higher power density than the conventional method at 42.5 ampere in primary current condition. Finally, the proposed method can be easily implemented in practical MEH applications.

## Acknowledgment

The authors would like to thank the technical support from Ferraris Inc. This work is patent pending by Ferraris Inc.

## References

[1] O. Menendez, F. A. Auat Cheein, M. Perez, and S. Kouro, “Robotics in Power Systems: Enabling a More Reliable and Safe Grid,” *IEEE Ind. Electron. Mag.*, vol. 11, no. 2, pp. 22–34, Jun. 2017, doi: 10.1109/MIE.2017.2686458.

[2] N. M. Roscoe and M. D. Judd, “Harvesting energy from magnetic fields to power condition monitoring sensors,” *IEEE Sens. J.*, vol. 13, no. 6, pp. 2263–2270, 2013, doi: 10.1109/JSEN.2013.2251625.

[3] R. H. Bhuiyan, R. A. Dougal, and M. Ali, “A miniature energy harvesting device for wireless sensors in electric power system,” *IEEE Sens. J.*, vol. 10, no. 7, pp. 1249–1258, 2010, doi: 10.1109/JSEN.2010.2040173.

[4] S. Paul, S. Bashir, and J. Chang, “Design of a Novel Electromagnetic Energy Harvester with Dual Core for Deicing Device of Transmission Lines,” *IEEE Trans. Magn.*, vol. 55, no. 2, pp. 2019–2022, 2019, doi: 10.1109/TMAG.2018.2873012.

[5] B. Park et al., “Analysis of magnetic energy harvester for inspection robot of power line using saturable inductor,” *IEEE Wireless Power Transfer Conference*, pp. 435–438, 2020, doi: 10.1109/WPTC48563.2020.929563.

[6] J. Zhou, B. Zhang, W. Xiao, D. Qiu, and Y. Chen, “Nonlinear Parity-Time-Symmetric Model for Constant Efficiency Wireless Power Transfer: Application to a Drone-in-Flight Wireless Charging Platform,” *IEEE Trans. Ind. Electron.*, vol. 66, no. 5, pp. 4097–4107, 2019, doi: 10.1109/TIE.2018.2864515.

[7] B. H. Choi, V. X. Thai, E. S. Lee, J. H. Kim, and C. T. Rim, “Dipole-Coil-Based Wide-Range Inductive Power Transfer Systems for Wireless Sensors,” *IEEE Trans. Ind. Electron.*, vol. 63, no. 5, pp. 3158–3167, 2016, doi: 10.1109/TIE.2016.2517061.

[8] B. Park *et al.*, “The Magnetic Energy Harvester with Improved Power Density Using Saturable Magnetizing Inductance Model for Maintenance Applications near High Voltage Power Line,” *IEEE Access*, vol. 9, pp. 82661–82674, 2021, doi: 10.1109/ACCESS.2021.3085989.

[9] B. Park *et al.*, “Optimization design of toroidal core for magnetic energy harvesting near power line by considering saturation effect,” *AIP Adv.*, vol. 8, no. 5, 2018, doi: 10.1063/1.5007772.

[10] L. Du, C. Wang, X. Li, L. Yang, Y. Mi, and C. Sun, “A novel power supply of online monitoring systems for power transmission lines,” *IEEE Trans. Ind. Electron.*, vol. 57, no. 8, pp. 2889–2895, 2010, doi: 10.1109/TIE.2009.2037104.

[11] J. Moon and S. B. Leeb, “Analysis Model for Magnetic Energy Harvesters,” *IEEE Trans. Power Electron.*, vol. 30, no. 8, pp. 4302–4311, 2015, doi: 10.1109/TPEL.2014.2357448.

[12] Y. Zhuang *et al.*, “Improving current transformer-based energy extraction from ac power lines by manipulating magnetic field,” *IEEE Trans. Ind. Electron.*, vol. 67, no. 11, pp. 9471–9479, 2020, doi: 10.1109/TIE.2019.2952795.

[13] M. J. Vos, “A Magnetic Core Permeance Model for Inductive Power Harvesting,” *IEEE Trans. Power Electron.*, vol. 35, no. 4, pp. 3627–3635, Apr. 2020, doi: 10.1109/TPEL.2019.2933133.

[14] C. Y. Lim, Y. Jeong, K. W. Kim, F. S. Kang, and G. W. Moon, "A High-Efficiency Power Supply from Magnetic Energy Harvesters," *2018 Int. Power Electron. Conf. IPEC-Niigata - ECCE Asia 2018*, pp. 2376–2379, 2018, doi: 10.23919/IPEC.2018.8507990.
[15] Samwha Electronics, "Mn-Zn power material," PL-7 datasheet, 2021.
[16] IEEE, "*IEEE* Standard for Test Procedures for Magnetic Cores," IEEE Power Electronics Society Sponsored by the Electronics Transformer Technical Committee, 1992.
[17] R. Moghe, F. C. Lambert, and D. Divan, "Smart stick-on sensors for the smart grid," *IEEE Trans. Smart Grid*, vol. 3, no. 1, pp. 241–252, 2012, doi: 10.1109/TSG.2011.2166280.
[18] C. Song *et al.*, "EMI Reduction Methods in Wireless Power Transfer System for Drone Electrical Charger Using Tightly Coupled Three-Phase Resonant Magnetic Field," *IEEE Trans. Ind. Electron.*, vol. 65, no. 9, pp. 6839–6849, 2018, doi: 10.1109/TIE.2018.2793275.

**BUMJIN PARK** received the B.S degree in Electrical Engineering from Chungnam National University, Daejeon, South Korea, in 2015 and the M.S. and Ph.D degrees in the Cho Chun Shik Grauate School of Green Transportation, Korea Advanced Institute of Science and Technology(KAIST), Daejeon, South Korea, in 2017 and 2022, respectively. He is currently Staff Engineer with Samsung Electronics, Suwon, South Korea, where he is in charge of power component design in wireless charging system.

**SUNGRYUL HUH** received the B.S degree in Electrical Engineering from Incheon National University, Incheon, South Korea, in 2018 and the M.S. degree in the Cho Chun Shik Grauate School of Mobility, Korea Advanced Institute of Science and Technology(KAIST), Daejeon, South Korea, 2020. He is currently working toward the Ph.D. degree in KAIST, Daejeon, South Korea. His research interest focuses on wireless power transfer system design for mobile device.

**HAERIM KIM** received the M.S. degree in the Cho Chun Shik graduate school of green transportation in 2019 from the Korea Advanced Institute of Science and Technology (KAIST), Daejeon, South Korea, where she is currently pursuing the Ph.D. degree. Her current research interest include the WPT.

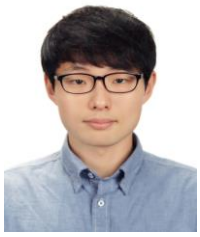

**JONGWOOK KIM** received the M.S. degree in the Cho Chun Shik graduate school of green transportation in 2017 from the Korea Advanced Institute of Science and Technology, Daejeon, South Korea, where he is currently working toward his Ph.D. degree. His current research interest include the WPT.

**YUJUN SHIN** received the B.S degree in Electrical Engineering from Inha University, Incheon, South Korea, in 2016 and the M.S. degree in the Cho Chun Shik Grauate School of Green Transportation, Korea Advanced Institute of Science and Technology, Daejeon, South Korea, 2018. He is currently working toward the Ph.D. degree in Korea Advanced Institute of Science and Technology, Daejeon, South Korea. His research interest focuses on wireless power transfer system design for electric vehicle.

**SEONGHO WOO** received the B.S. degree in Electrical Engineering from Kyungpook National University, Korea, in 2019, and the M.S. degree in 2021 from CCS Graduate School of Green Transportation from the Korea Advanced Institue of Science and Technology (KAIST), Daejeon, South Korea, where he is currently working toward the Ph.D. degree. His research interests include electromagnetic interference and wireless power transfer.

**DONGWOOK KIM** (Member, IEEE) received the M.Sc. and Ph.D. degrees in green transportation from the Korea Advanced Institute of Science and Technology (KAIST), Daejeon, South Korea, in 2016, and 2019, respectively. He is currently an Assistant Professor with the Department of Automotive Engineering, Yeungnam University, Gyeongsan, South Korea. His research interests include wireless power transfer system in microrobots, implantable devices, and electric vehicles.

**KI-BUM PARK** received B.S., M.S., and Ph.D. degrees in electrical engineering from the Korea Advanced Institute of Science and Technology (KAIST), Daejeon, Korea, in 2003, 2005, and 2010, respectively. After 9 years of industry experience in ABB Switzerland, he is currently with KAIST, South Korea, as an Associate Professor. His research interests include power electronics system for transportation electrification, renewable integration, and wireless power transfer.

**OKHYUN JEONG** received the B.S.,M.S., and Ph.D. degrees in elec-tronic engineering from the Sogang University, Seoul, South Korea, in 1982, 1985, and 1996, respectively. He is currently an Associate Professor of Department of Electronic engineering, Sogang University since March 2012. His research interest includes power consumption and thermal management model of mobile IOT device and wireless power charging system design for wearable robot.

**JA-IL KOO** received the M.S., and Ph.D degree in electrical engineering Department from the Korea Advanced Institute of Science and Technology, Daejeon, South Korea in 1987 and 1991, respectively. He is currently CEO of Ferraris Inc, located at Las Vegas NV USA and has been developed Magnetic Harvesting Device and System for last more than 10 years. He has more than 10 Magnetic harvesting related international Patents and published more than 10 related papers.

**SEUNGYOUNG AHN** (Senior Member, IEEE) received the B.S., M.S., and Ph.D. degrees from the Korea Advanced Institute of Science and Technology (KAIST), Daejeon, South Korea, in 1998, 2000, and 2005, respectively, all in electrical engineering. From 2005 to 2009, he was a Senior Engineer with Samsung Electronics, Suwon, South Korea, where he was the incharge of high-speed board design for laptop computer systems. He is currently a Professor with CCS Graduate School of Green Transportation, KAIST, Daejeon. His current research interests include wireless power transfer system design and electromagnetic compatibility design for electric vehicle and high-performance digital system.